Environmental Pollution 347 (2024) 123708

Contents lists available at ScienceDirect

Environmental Pollution

journal homepage: www.elsevier.com/locate/envpol

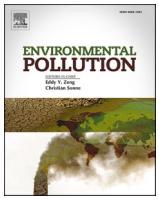

Long term trends in source apportioned particle number concentrations in Rochester NY☆

Philip K. Hopke [a,b,*], Yunle Chen [a], David C. Chalupa [c], David Q. Rich [a,c]

[a] Department of Public Health Sciences, University of Rochester School of Medicine and Dentistry, Rochester, NY, 14642, USA
[b] Institute for a Sustainable Environment, Clarkson University, Potsdam, NY, 13699, USA
[c] Department of Environmental Medicine, University of Rochester School of Medicine and Dentistry, Rochester, NY, 14642, USA

ARTICLE INFO

Keywords:
Particle number size distributions
Source-specific particle number concentrations
Trends
Traffic
Nucleation
Regulations

ABSTRACT

During the past two decades, efforts have been made to further reduce particulate air pollution across New York State through various Federal and State policy implementations. Air quality has also been affected by economic drivers like the 2007–2009 recession and changing costs for different approaches to electricity generation. Prior work has focused on particulate matter with aerodynamic diameter ≤2.5 μm. However, there is also interest in the effects of ultrafine particles on health and the environment and analyses of changes in particle number concentrations (PNCs) are also of interest to assess the impacts of changing emissions. Particle number size distributions have been measured since 2005. Prior apportionments have been limited to seasonal analyses over a limited number of years because of software limitations. Thus, it has not been possible to perform trend analyses on the source-specific PNCs. Recent development have now permitted the analysis of larger data sets using Positive Matrix Factorization (PMF) including its diagnostics. Thus, this study separated and analyzed the hourly averaged size distributions from 2005 to 2019 into two data sets; October to March and April to September. Six factors were resolved for both data sets with sources identified as nucleation, traffic 1, traffic 2, fresh secondary inorganic aerosol (SIA), aged SIA, and O3-rich aerosol. The resulting source-specific PNCs were combined to provide continuous data sets and analyzed for trends. The trends were then examined with respect to the implementation of regulations and the timing of economic drivers. Nucleation was strongly reduced by the requirement of ultralow (<15 ppm) sulfur on-road diesel fuel in 2006. Secondary inorganic particles and O_3-rich PNCs show strong summer peaks. Aged SIA was constant and then declined substantially in 2015 but rose in 2019. Traffic 1 and 2 have steadily declined bur rose in 2019.

1. Introduction

Airborne particulate matter is the largest environmental cause of excess mortality and morbidity (GBD, 2020) resulting in an estimated 7 million deaths per year (WHO, 2021). The primary focus of health studies and resulting regulations has been on particulate matter mass concentrations in various aerodynamic size fractions (≤2.5 μm or ≤ 10 μm). However, there are also indications of the health impacts of smaller sized particles, the ultrafine particles (UFPs) with mobility sizes below 100 nm.[1] Initial studies of the health impacts of UFPs were begun in the 1990s using animal toxicological studies (e.g., Oberdörster et al., 1992). Utell and Frampton (2002) explored the effects of generated ultrafine particles on humans in clinical studies. Ambient particle number concentrations (PNCs) have been associated with cardiovascular effects. For example, an increased rate of ST-elevation myocardial infarction (STEMI) associated with increased UFP concentrations in the previous hour among adults in Rochester, NY from 2005 to 2016 (Wang et al., 2019). In a further study in Rochester, Yount et al. (2023) reported that the association seen in 2014–2016 was no longer observed in 2017–2019 likely due to changing compositions. WHO (2021) reviewed the effects of UFPs but concluded that there was not yet sufficient information to set health-protective concentration guidelines but recommends continued studies.

Trechera et al. (2023) reviewed particle number concentrations

☆ This paper has been recommended for acceptance by Prof. Pavlos Kassomenos.

* Corresponding author. Department of Public Health Sciences, University of Rochester School of Medicine and Dentistry, Rochester, NY, 14642, USA.
E-mail address: phopke@clarkson.edu (P.K. Hopke).

[1] The definitions for all of the acronyms used in this report are provided in a glossary in the supplemental material.

https://doi.org/10.1016/j.envpol.2024.123708
Received 5 January 2024; Received in revised form 16 February 2024; Accepted 2 March 2024
Available online 3 March 2024

across 26 sites in Europe and in Rochester. Prior studies have been performed in a number of locations on the source apportionment of particle number size distributions (PNSDs) (Hopke et al., 2022). However, there are relatively limited studies of PNCs and PNSDs particularly long-term studies in urban locations that would permit analysis of trends in PNC or size-specific PNCs that would be derived from source apportionment of PNSDs.

As part of the ongoing studies of UFPs at the University of Rochester, a particle size distribution monitoring system was established in November 2001 on the main fire station in downtown Rochester NY in conjunction with the New York State Department of Environmental Conservation's (NYS DEC) criteria pollutant monitoring station at that location. In 2004, the site was closed, and the instruments were moved to the current NYS DEC site on the eastern side of the city (lat: 43.146183°N; lon: 77.54215°E). However, instrument problems precluded starting measurements at this location until January 2005, and they have continued there to the present. The resulting data have been the subject of a number of publications describing the characteristics of the PNCs (Jeong et al., 2004, 2006; Wang et al., 2011a), trends in PNCs in various size ranges (Masiol et al., 2018; Chen et al., 2022), and PNC sources (Ogulei et al., 2007a; Kasumba et al., 2009; Squizzato et al., 2019).

One of the major goals of this long-term monitoring was to assess the changes in PNCs related to changes in source emissions over time driven by implementation of regulations or through changes driven by economic changes and events such as the 2007–2009 recession. Similar trends studies has been done by Chen et al. (2023) on all of the criteria pollutants measured across New York State at all of the NYS DEC monitoring sites. A table outlining the regulations and economic drivers is provided as Table S1 in the Supplemental Material. However, it has previously not been possible to explore the trends in source-specific PNCs because of software limitations described by Hopke et al. (2023). As they described in that paper, there is now an approach to use the multilinear engine (ME-2) (Paatero, 1999) including the diagnostic tools presented in Paatero et al. (2014) to analyze large data set. Thus, it is now possible to analyze a much larger data set to provide source apportioned PNC that can be used in trend analyses. The objectives of this work were then to apportion the PNC values from 2005 to 2019 to sources, to analyze the trends in the source-specific PNCs, and to relate these trends to likely causes including implementation of regulations and changes in emissions resulting from economic drivers.

2. Data and methods

2.1. Measurements

Measurements were made at the NYS DEC site in Rochester, NY (Lat: 43.14501°N: Lon: 77.55728°W) as shown in Fig. 1. A wider view of Rochester showing the site locations is provided in Fig. S1 of the supplemental material. The particle size distributions from 10 to 500 nm were made from 2005 to August 2018 using a TSI model 3071 differential mobility analyzer (DMA) and a TSI model 3010 condensation particle counter (CPC). In mid-August 2018, this system was replaced with a TSI Model 3082 classifier with a Model 3081a long DMA and a TSI model 3750 CPC. At this site, NYS DEC also measures hourly values of $PM_{2.5}$, CO, SO_2, and O_3 using standard regulatory monitors. In July 2008, a Magee Scientific AE21 2-wavelength aethalometer was added to measure light absorbing carbon at 370 and 880 nm. The resulting BC (880) and BC(370) were used to calculate DC (BC(370)-BC(880)) as described by Wang et al. (2011b).

2.2. Positive Matrix Factorization analyses

The data set covering the period of 2005–2019 consists of total PNC, PNC values for 54 geometrically sized bins with midpoint diameters from 11.1 to 470 nm, $PM_{2.5}$, CO, SO_2, O_3, BC(880) and DC. The resulting data set consisted of 104,311 hourly values of 60 variables or 6,258,660 data points. Uncertainties in the PNC values were estimated using the approach of Ogulei et al. (2007a) and Squizzato et al. (2019). Uncertainties for the ancillary variables from the manufacturers' specification and the approach of Polissar et al. (1998). As noted in Hopke et al. (2023), the ME-2 program has a limit to the number of equations it can

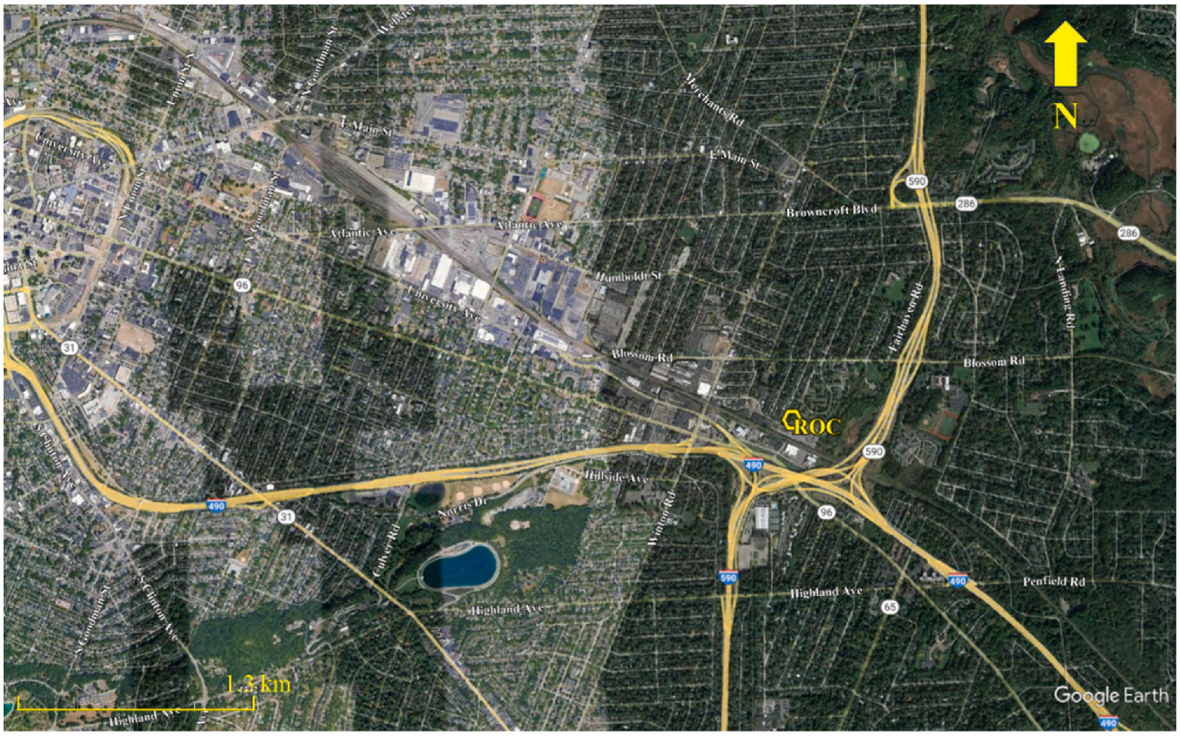

Fig. 1. Google Earth view of the eastern side of Rochester, NY showing the NYS DEC monitoring site (ROC).

handle and for these data that represents a limit of less than 6 million data points. Thus, it was not possible to analyze the entire data set in a single analysis. Also previously, Zhou et al. (2004, 2005) and Ogulei et al. (2007a) found that sufficient changes in the size distribution profiles during the year due to changing atmospheric chemistry warranted separating the year into subsets. Thus, the data were divided into 2 subsets representing cold (October to March) and warm (April to September) periods.

Since factor analysis methods like PMF depend on "edge" points in the data set where one or more sources have little or no contribution to that sample, meteorological variations can raise or lower concentrations depending on the dispersion conditions. Prior work has shown that dispersion normalization can substantially improve the source apportionments particularly for hourly PM data (Dai et al., 2020, 2021a) and PNC size distributions (Dai et al., 2021b; Chen et al., 2022). Dispersion normalization (DN) is based on the ventilation coefficient, VC, that is calculated as the product of the mixed layer height times the average wind speed during the sampling period. Hourly wind speeds were obtained from the Frederick Douglas Rochester International Airport National Weather Service monitoring site (KROC) via the National Centers for Environmental Information (NCEI, 2023). Rochester has no of mixed layer heights monitoring. Thus, hourly mixed layer heights were obtained using modeled values available from the ERA5 hourly data on single levels from 1940 to present website (https://cds.climate.copernicus.eu/cdsapp#!/dataset/reanalysis-era5-single-levels?tab=form). DN involves normalizing each sampling interval to have the same VC as the mean VC of the whole data set. Thus, each hourly data set is multiplied by VC_{mean}/VC_i where i is the index for this specific sampling interval. Each of the 2 DN data sets were analyzed using ME-2 to make the PMF analyses as well as providing the displacement (DISP) and bootstrap (BS) outputs (Paatero et al., 2014). As noted by Hopke et al. (2023), the time to perform a BS-DISP analysis is too long (~75 days) to be practical and thus, it was not performed.

The resulting source-specific PNC concentrations were then unnormalized by multiplying the resolved values by VC_i/VC_{mean}. These values were then analyzed using the "timeVariation" routine of the 'openair' package (Carslaw and Ropkins, 2012). The wind speed and directional data were from KROC (NCEI, 2023) were combined with the PMF results to provide conditional bivariate probability function (CBPF) plots (Uria-Tellaetxe and Carslaw, 2014) using 'openair.'

2.3. Trend analyses

Three different trend analyses were performed on the complete time series for each of the resolved factors that was developed by combining the results of the two seasonal PMF analyses. The trend analyses were done on monthly average values of the source-specific PNC values. Monotonic trends in the source-specific PNCs were assessed by calculating the Thiel-Sen slope (Theil, 1950; Sen, 1968) using the routine available in 'openair.' This method calculates the median of the slopes between all pair of points in the time series and its associated confidence interval. The second approach, seasonal trend decomposition based on loess (STL) (Cleveland et al., 1990), separates a continuous smoothed trend from the seasonal variation and calculates the residual after subtracting the two time-series from the inputted source-specific PNC values. Missing monthly values were imputed using a Kalman filter. The STL analyses were performed using the 'smoothTrend' procedure in 'openair.' Finally, piece-wise regression was applied to explore breaks in the slope of the time series that might have reflected the implementation of a policy or economic influence. This analysis was implemented in the 'segmented' package in R (Muggeo, 2003; 2008).

3. Results and discussion

Factor solutions from 5 to 8 factors were examined for both data subsets. The 6-factor solution was chosen as the best result. It fit the data adequately as shown by the scaled residual distributions, and the profiles were easily interpretable for both data sets as Nucleation, Traffic 1, Traffic 2, Fresh Secondary Inorganic Aerosol (FSIA), Aged Secondary Inorganic Aerosol (ASIA), and O_3-Rich, similar to what had been resolved in prior analyses (e.g., Squizzato et al., 2019). The 5-factor solution did not adequately fit the data as shown by the scaled residual distributions. The 7-factor solution had less compatible profiles between the warm and cold periods and thus, were harder to interpret. The 8-factor solution clearly showed factor splitting and was discarded.

The PNC portions of the profiles have been normalized by the total PNC values for each factor, so they are unitless fractions of the total PNC in each size bin. The PNC contributions have been normalized by the same PNC contributions for each factor and then unnormalized for dispersion as described above. The ancillary variable have not been normalized and are concentrations in their native measurement units. The profiles and contribution plots for the 6-factor solution are shown in Fig. 2 (cold) and 3 (warm). The apportionment results including the average PNC and percent contribution to the total for the warm, cold, and whole year periods are provided in Table 1. Each of the factors will be discussed separately with respect to the likely physical sources and atmospheric processes that led to the size distribution and concentrations that have been observed.

3.1. Nucleation

This factor profile shows a peak for the winter data at 17 nm, while the summer mode peak is at 16 nm. Both represent most of the PNCs below 20 nm. In Table 1, Nucleation is seen to contribute 18% of the PNCs as the 4th largest particle source. Given the colder temperatures in winter, a slightly larger size during the cold period might be the result of lower vapor pressures for semivolatile constituents. It is similar to what has been reported in prior apportionments of PNC size distributions (Dai et al., 2021b; Hopke et al., 2022 and references therein). The profile for the other pollutants shows small contributions to CO, SO_2, and BC with very little O_3, DC, or $PM_{2.5}$, consistent with motor vehicle emissions and photochemical new particle formation events.

This factor represents a combination of both direct emissions from combustion sources including vehicular traffic along the major roads in the vicinity of the site (Fig. 1), the diesel-powered railroad that is about 100 m from the monitoring site, and new particle formation (NPF) events as suggested by the time series of diel patterns shown in Fig. S2. In the early years (2005 and 2006), there was a clear morning rush hour peak at 7–8 a.m. local time that is from vehicular traffic. There was also a broader early afternoon peak at approximately 1 p.m. local time that is ascribed to photochemically induced new particle formation. These peaks diminish over time until 2015 with the rush hour peak becoming less distinct and the NPF processes becoming dominant. However, beginning in 2015 and continuing until 2019, the morning rush hour peak grows relative to the NPF activity. The relatively flat pattern from late morning through midnight in recent years may be due to the train traffic along the main line tracks near to the monitoring site where freight trains run frequently.

The day-of-the-week time patterns as a function of year are shown in Fig. S3. Initially, there was a strong decline in concentrations for Saturday and Sunday that diminishes as the concentrations decrease and the relative contribution of vehicular traffic diminishes. However, the Saturday/Sunday drop returns more clearly in 2017 as the influence of traffic increased as seen in the diel patterns. The monthly mean and associated confidence intervals are shown in Fig. S4 and depict similar trends downward at the beginning of the study period and rising during the last several years. In the early part of the period, there were peaks in winter when colder temperatures support more heterogenous nucleation of semivolatile emissions onto co-emitted particles with smaller summer photochemical peaks. From 2013 through the end of the period, seasonal patterns were much less discernible. As can be seen in Fig. 4, there were data gaps from July to September 2006 and September to

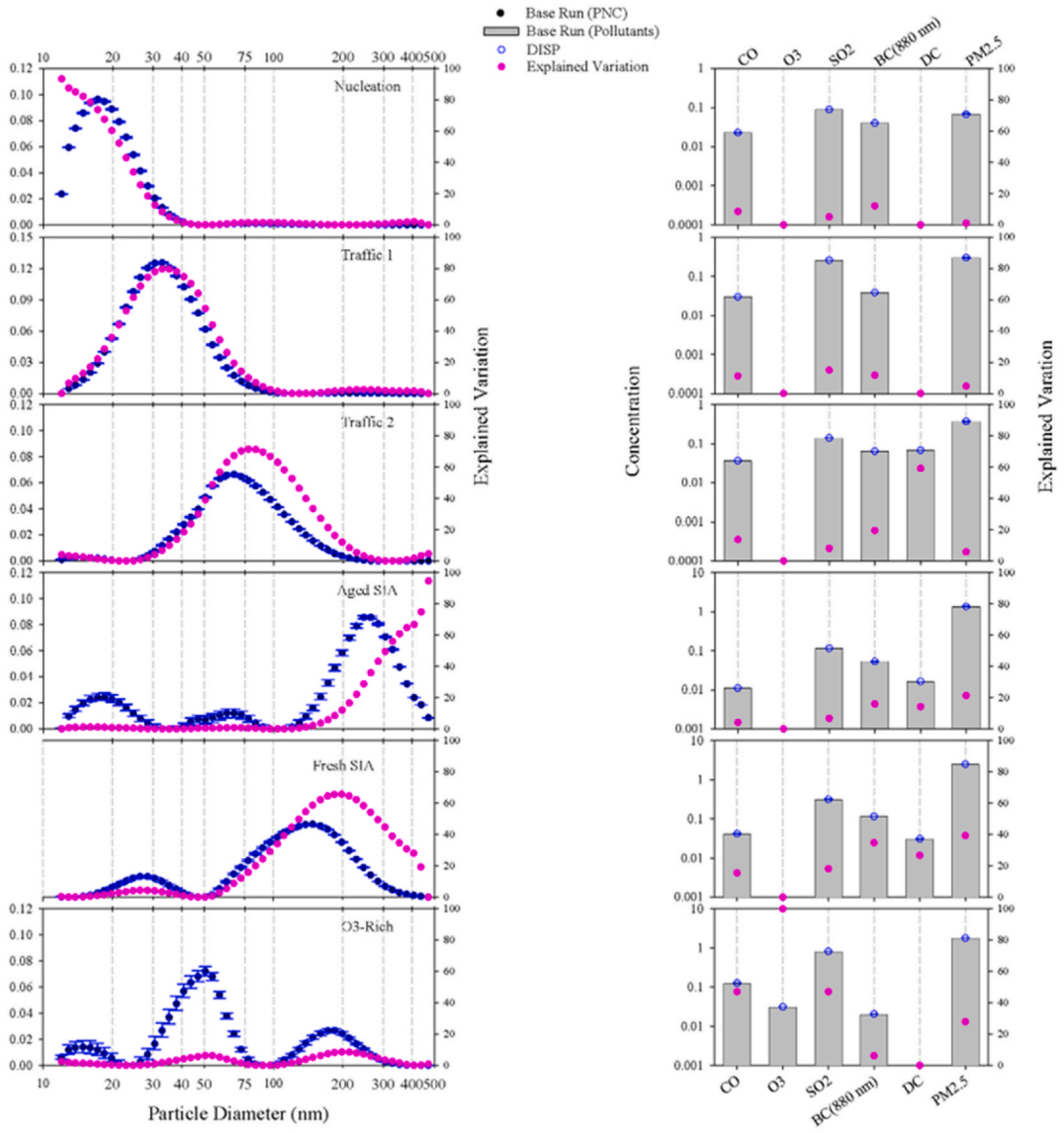

Fig. 2. Source profiles for the cold (left) and warm(right) period analyses.

Table 1
Results of the PNC apportionments by season and whole year.

Source	Warm Season		Cold Season		Whole Year	
	Mean PNC	% Contribution	Mean PNC	% Contribution	Mean PNC	% Contribution
Nucleation	744.4	15.50	975.6	20.37	861.7	17.96
Traffic 1	1234.3	25.70	1892.6	39.51	1568.4	32.69
Traffic 2	1220.1	25.40	1265.2	26.41	1243.0	25.91
Aged SIA	123.4	2.57	70.0	1.46	96.3	2.01
Fresh SIA	1248.1	25.98	78.3	1.63	154.7	3.23
O3-Rich	233.5	4.86	508.8	10.62	873.0	18.20

December 2012 where the SMPS was not operating because it was being repaired and several other smaller gaps occurred due to instrumental interruptions. The overall data capture rate was around 83% over the 15-year period.

The formal trend analyses are shown in Fig. S5, and the numerical values are presented in Table 2. For Nucleation, there is a sharp drop from 2006 to 2007 and a rise from 2014 to 2019. The drop in 2006–2007 may be attributable to the requirement that 80% of the on-road diesel fuel in the United States be ultralow (<15 ppm) as of October 1, 2006. Thus, much less SO_2 and SO_3 were emitted from the on-road heavy-duty diesel (HDD) vehicles as the fuel S content changed. The SO_2 can oxidize to form sulfuric acid that will nucleate with ammonia or amides. Further declines occurred as more post-2007 HDD vehicles equipped with particle traps entered the fleet and post 2010, when NOx controls were added to new HDD vehicles. Non-road diesel fuel S content was required to move to ultralow S beginning in 2010 and completed by the end of 2013. New York required all distillate fuels sold in the state after July 1, 2012 to be ultralow S.

The upward trend beginning in 2014, is likely the result of the substantial reduction in $PM_{2.5}$ that was occurring from 2010 onward (Chen

Table 2
Results of the trend analyses.

Factor	Theil-Sen Slope		Segmented Slope	
	# cm-3 yr-1	% yr-1	Slope (# cm-3 yr-1)	Period
Nucleation	−6 [-30, 17]	−0.79 [-3, 2.69]	−784 [-893, −675]	01/2005-05/2006
			−65 [-73, −58]	05/2006-11/2014
			231 [215, 247]	11/2014-12/2019
Traffic 1	−62 [-84, −40]	−3.33 [-4.16, −2.37]	−202 [211, −193]	01/2005-07/2011
			5 [-2, 13]	07/2011-11/2018
			867 [731, 1002]	11/2018-12/2019
Traffic 2	−62 [-77, −45]	−3.72 [4.35, −2.99]	−192 [-202, −182]	01/2005-07/2011
			2 [-6, 10]	07/2011-12/2018
			652 [504, 800]	12/2018-12/2019
Aged SIA	−8 [-10, −6]	−5.27 [-5.91, −4.47]	0 [-2, 1]	01/2005-12/2011
			32 [9, 56]	12/2011-12/2012
			−25 [-27, −23]	12/2012-10/2018
			105 [86, 123]	10/2018-12/2019
Fresh SIA	−28 [-45, −11]	−3 [-4, −1]	102 [89, 115]	01/2005-03/2008
			−145 [-157, −132]	03/2008-08/2011
			2 [-2, 6]	08/2011-08/2018
			321 [276, 366]	08/2018-12/2019
O3 Rich	3 [0, 6]	2.31 [-0.16, 5.60]	84 [78, 90]	01/2005-10/2006
			−3 [-3, −3]	10/2006-12/2019

et al., 2023). The shut-down of many coal-fired power plants during the 2007–2009 recession reduced SO_2 emissions and the low cost of fracked natural gas meant a substantial shift in electricity generation to new combine cycle natural gas turbines and renewables as described by Squizzato et al. (2018). Thus, the reduction in accumulation mode sulfate particles substantially reduced the condensational sink such that new particle formation became possible (McMurry and Friedlander, 1979).

In addition, the shift in light-duty spark-ignition vehicles from port fuel injection (PFI) to gasoline direct injection (GDI) beginning in 2007 meant that by 2014, a substantial fraction of the fleet was using GDI engines. From 2010 to 2014, gasoline in the United States was being reformulated to reduce its benzene content. To maintain the performance of the gasoline vehicles, intermediate volatility organic compounds were used as replacements (Zhao et al., 2014). As a result of the combination of changes in engine technology and gasoline constituents, more secondary organic aerosol (SOA) was being produced based on the studies of Zhao et al. (2015, 2016, 2018).

To further investigate the sources of nucleation mode particles, the CBPF plots by season and year are presented in Figs. S6–S9. These plots present the probabilities of sources to be in the direction (angular dimension) and associated with wind speed (radial direction). Lower wind speeds are normally associated with more local sources while higher wind speeds suggest more distant sources. In the early years, the source areas throughout the year were to the south of the site where the major highways are situated. However, in the last 2 years, there was a shift to the northwest for summer and autumn when there were the highest probabilities. Northwest is the direction of the railroad tracks leading to a relatively large switch yard (Fig. S1). Unpublished studies has found high concentrations of black carbon coming from that rail yard and it is likely that the diesel engines were a source of nucleation mode particles and condensable organic compounds. Kittelson et al. (2002, 2004, 2006a) and Ogulei et al. (2007b) report measurements of nucleation mode particles as part of a multimodal distribution present in diesel engine exhaust.

3.2. Traffic 1

These profiles have single modes at 28 nm (warm) and 31 nm (cold) and similar profiles have been reported in many studies. The ancillary variables in this profile are also CO, SO_2, and BC with little or no O_3, DC, or $PM_{2.5}$. Over the whole year, Traffic 1 provided the highest contributions to the measured PNC representing about 33% of the PNC. This profile has consistently been assigned to spark-ignition vehicles by a number of studies (Hopke et al., 2022 and references therein) and the assignment is supported by measured distributions reported by Kittelson et al. (2006b) and Ogulei et al. (2007b). Such vehicles would also expel condensable gases that would have nucleated and been assigned to Nucleation. Fig. S10 presents the annual average diel patterns by year in which a morning rush hour pattern can be discerned across all of the years. There were also relatively flat values through the late morning and early afternoon with evening peaks in recent years. A slow but continuous trend downward can be observed across the whole study period.

The day-of-the-week plot (Fig. S11) shows a low Sunday pattern but somewhat erratic low values on Saturday that varied from year to year. There is again a slow decline in traffic 1 PNC through 2013 when they became relatively constant. The month-of-the-year plot in Fig. S12 shows winter high values. Although the conventional explanation would be poorer dispersion conditions due to lower mixed layer heights and wind speeds, Rochester has anomalously higher winds in the winter compared to many locations so there is actually more dispersion in winter than in summer (Fig. S13). The time variations in VC values were relatively similar from year to year as shown in Fig. S14. There may be increase cold starts in the winter leading to the increased winter concentrations as well as morning rush hour when the VC values were low.

The trend analyses are depicted in Fig. S15 with the numerical details in Table 2. There was a slow decline from 2005 to 2012, likely due to the increased penetration of Tier 2 vehicles into the on-road fleet with a rise in 2018 and 2019. There is a dip in the STL plot in 2012 where there was a substantial loss of data from instrument failure. The trends in $PM_{2.5}$ apportioned to gasoline vehicles reported by Chen et al. (2024) indicated an increase beginning in 2015. Since there are weak correlations between PNC and $PM_{2.5}$ (Jeong et al., 2004), there may have been substantial coagulation of the locally emitted Traffic 1 particles with the regional secondary inorganic aerosol that represented the bulk of the $PM_{2.5}$ surface area up to around 2017 as discussed above for Nucleation.

The seasonal CBPF plots (Figs. S16–S19) generally show the areas of maximum probability to be to the south of the site in the direction of the major roadways and the railroad. The decline in Traffic 1 PNC can be seen with the decline of the probabilities across the study period. In the summer (JJA) in recent years, there are areas of higher probability to the northwest in the direction of the rail yard.

3.3. Traffic 2

Traffic 2 is characterized by a mode centered around 66 nm in winter and 75 nm in summer. This profile has the opposite seasonal behavior compared to Nucleation and Traffic 1. The ancillary variables in this profile are CO, O_3, SO_2, BC and DC but with no $PM_{2.5}$. This source has been alternatively assigned as aged traffic particles (Zhou et al., 2004, 2005) or diesel vehicle emissions (Kasumba et al., 2009; Squizzato et al., 2019; Dai et al., 2021b). This peak is similar to the larger mode in the

measured distributions of Kittelson et al. (2002, 2004, 2006a) and Ogulei et al. (2007b). The diel patterns are shown in Fig. S20. These patterns are distinctly different from Traffic 1 with a strong evening peak up to midnight and a much weaker morning rush hour peak (7–9 a.m.). The day of the week variations are shown in Fig. S21. There is a much weaker or no drop in PNC on weekend days when compared to Traffic 1. Heavy-duty diesel (HDD) traffic in Rochester is a combination of long-haul trucks delivering or picking up loads in Rochester, local HDD vehicles, and the railroad. This combination appears to provide more uniform emissions with similar evening peaks on all evenings as seen in the hour of week plots (not shown). The monthly patterns are presented in Fig. S22. In the early years, there were clear peaks in the winter. The periods with the highest concentration were in the evening (Fig. S20) even after adjusting for dispersion since at that time VC values are below average Fig. S14b). These winter peaks declined across the study period as the combination of cleaner on- and non-road diesel fuel replaced the traditional fuel and there was continuous penetration of new HDD vehicles with particle traps and then selective catalytic reduction systems for particle and NOx controls.

The trend analyses are shown in Figure F23. The STL plot shows a sharp drop in 2005–2006 and then a longer-term, lower slope decline up to 2012. These decrements may be associated with the HDD rules that introduced ultralow S fuel in 2006, particle trapped new vehicles in 2007, and NOx controls in 2010. There again is a 2013 dip as in Traffic 1 with no known cause. Over the past decade, Traffic 2 has been relatively constant but with a rise in 2018 and 2019. It is not clear why there is this rise since more of the pre-2007 should be rotating out of the fleet. There was an increase in economic activity beginning in 2017 and that may have resulted in higher HDD vehicle traffic. However, there is also an indication of leaking from aging catalytic regenerative traps (Yang et al., 2016; Preble et al., 2019) and it may be that it contributes to the Traffic 2 PNC rise.

Figs. S24–S27 present the CBPF plots for Traffic 2. The patterns in the early years suggest emissions from the west of the monitoring site generally at low wind speeds suggesting sources near the monitor. Thus, there appears to be more influence of the railroad and potentially the rail switch yard. There is no indication from the 2018 or 2019 CBPF plots suggesting reasons for the rise in the most recent years. Examination of the trends in source-specific $PM_{2.5}$ from diesel vehicles (Chen et al., 2024) show mixed recent year trends across New York with some increasing and some decreasing so it appears that the rise in Rochester may be the result of increased local diesel activity.

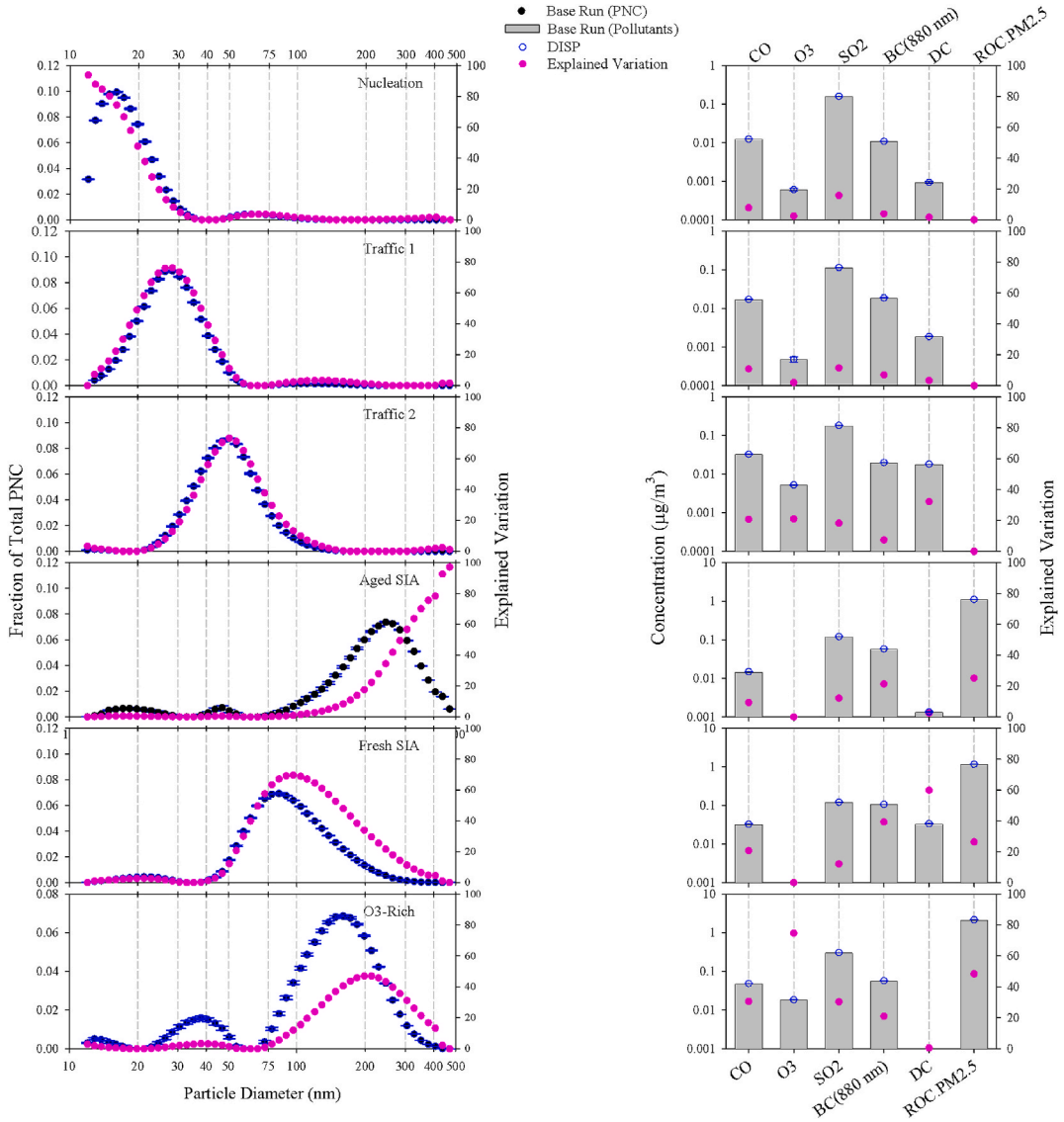

Fig. 3. Source profiles for the cold (left) and warm(right) period analyses.

3.4. Aged Secondary Inorganic Aerosol

This profile represents the largest size particles that were measured with the SMPS (Figs. 2 and 3). Ancillary variables include SO_2, BC, and about one-third of the $PM_{2.5}$. In prior studies, the winter profile was typically labeled as secondary nitrate. The annual average diel patterns by year, month-of-year and day-of-week are presented in Figs. S28–S30, respectively. There is a significant drop in PNC between 2014 and 2015 that continues for the rest of the study period with another drop in 2019 as seen in the diel patterns (Fig. S28) and the day-of-week (Fig. S29) plots. However, this factor represents a very low source of particles with values below 25 #/cm^3 so there is a large uncertainty in these values. The diel patterns show a weak traffic pattern that diminished after 2013. The day-of-week plot does not suggest any clear pattern as would be expected from a regional source. The month of the year plots shown in Fig. S30 generally show a summer peak with weak winter peaks. The summer peaks are attributed to secondary sulfate while the winter peak was expected to be largely secondary nitrate given the differences in formation rates between summer and winter.

To try to understand the apparent shift in concentration beginning in 2013, further analyses were made. There were closures of out-of-state coal-fired power plants including a number of shutdowns in Ontario beginning in 2009 and given the reduced demand for electricity during the 2007–2009 recession. Fig. 5 shows the SO_2 and NOx emissions in the United States from 2000 to 2020 (USEPA, 2023) as a result of various policy implementations and the 2007–2009 recession. There was a substantial decline in the SO_2 emissions in 2014 that extends to 2016. During this period, several coal-fired power plants in western NY were closed. The 816-MW Huntley plant in Tonawanda began reducing its output in 2015 going from 3192 tons of SO_2 in 2014 to 1158 tons in 2015 and closed completely in March 2016. The 627- MW plant in Dunkirk, NY was closed in January 2016 with only a small decrease in emissions between 2014 and 2015. Reductions in sulfate or nitrate PM were not observed in Rochester (Chen et al., 2024). Thus, the major reduction in larger particle sizes may be in part the result of reduced emissions in western NY. However, the origins of the full extent of the reduction are unclear. Given the reductions in local sources, it may be that given greater distances from the remaining SO_2 sources, there was an increase in particle sizes through additional cloud processing that increased the diameter of the particles, so they fell outside of the measurement range of the SMPS. John et al. (1990) reported that there were two size modes for the inorganic aerosol in the accumulation mode size range. The smaller mode with a peak at 0.2 ± 0.1 μm aerodynamic diameter, was assigned to be a condensation mode resulting from homogeneous

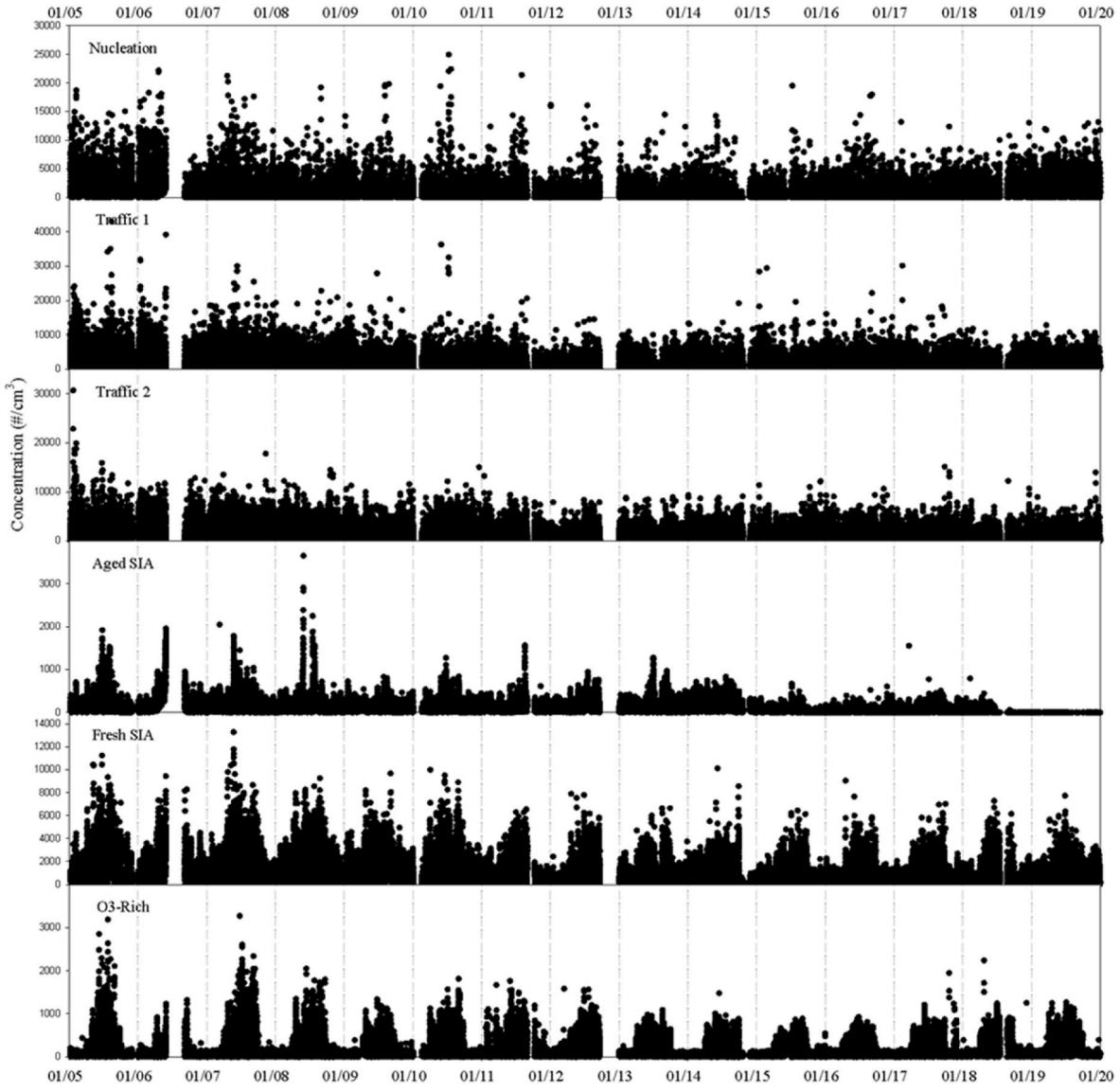

Fig. 4. Time series of contributions from each of the factors.

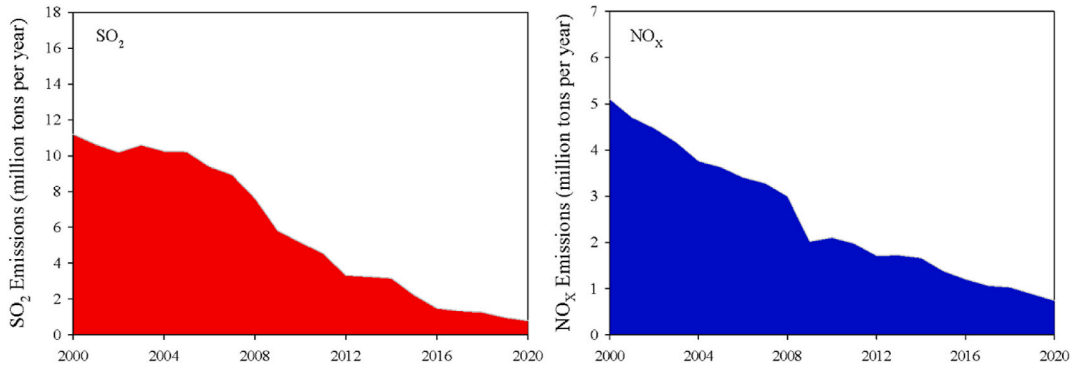

Fig. 5. United States total emissions of SO_2 and NOx from 2000 to 2020 as reported by the US EPA (2023).

oxidation of the precursor gases that nucleated to form the product particles. The larger mode at 0.7 ± 0.2 μm was assigned to be the result of a droplet mode in which additional material was accumulated leading to the larger particle size.

The trend results are shown in Fig. S31 that shows a general decline in the piecewise and STL analyses but with a small peak in early 2013 of unknown origin. There was a constant value through late 2018 with a rise during the last 14 months of the study period. There are no similar increases in 2019 in either secondary sulfate or nitrate PM (Chen et al., 2024). This factor was important in terms of representing the majority of PNC in sizes above 250 nm.

3.5. *Fresh Secondary Inorganic Aerosol*

This bimodal profile has a major mode around 150 nm with a minor mode in the range of 20–30 nm (Figs. 2 and 3). The winter major mode is larger than that in summer where the mode is in the 90–100 nm range. The colder temperatures in winter would lead to additional material condensation onto the particles leading to its larger size. It also may be augmented by non-secondary local building heating emissions that had been resolved in earlier studies (Kasumba et al., 2009; Squizzato et al., 2019). The diel patterns (Fig. S36) show higher concentrations and smoother results across the study period. There are clear peaks around midnight and in the morning around 6 a.m. The overnight peak supports the contribution from heating emissions. In addition, this factor had a high explained variation of DC, a marker of wood combustion (Wang et al., 2011b). The 6 a.m. peak is earlier than the morning rush hour seen in traffic diel patterns. Zhou et al. (2005) reported the possibility of nitrate nucleation around sunrise when temperatures are minimal, and photochemistry has just begun. The time around sunrise would be more likely to have relative humidity values around the deliquesce relative humidity for ammonium nitrate (~60%) (Wang et al., 2020). There are much sharper peaks in the early years with gradual diminution to around 2012 and relatively constant patterns to the end of the period.

There were mixed weekend day patterns with declines in some years and increases in other (Fig. S37). In the day-of-week results, there is also a sharp drop as in the Aged SIA concentrations, but in this case, it was between 2010 and 2011 with continued lower concentrations out to 2019. Again, there is not an obvious association of this drop with known changes in likely sources. The monthly variations for each year are presented in Fig. S38 showing strong peaks in each summer although the magnitude of the peaks declining relatively smoothly over time. The large summer peak suggests that the composition is likely to be sulfate.

The trend analyses in Fig. S39 show a relatively flat over all result with a wide variation in the monthly mean values. Fig. S38 showed strong summer peaks but they have been separated from the central emissions trends in the STL line. The piecewise analysis showing a rise in the early years, a decline until 2012, constant until 2019 and again a rise in 2019 similar to what was seen in several other concentration trends.

The CBPF plots (Figs. S40–S43) generally show higher probabilities centered on the south of the monitoring site at moderate wind speeds (5–10 m/s). There were higher seasonal values in different years although the highest values were typically in the early years in the winter and spring. The summer high probabilities tended to be more southwesterly in the early years. In the first several years, there was still high higher S in on-road and non-road diesel fuel and thus, the potential for local formation of particles as seen by Sun et al. (2011) in 2009 in New York City. However, these events were observed at midday when photochemistry was highest while the observed pattern here was at midnight suggesting primary emissions of SO_3 likely coming from diesel locomotives prior to the requirement of ultralow S non-road diesel fuel.

3.6. *O_3-rich*

The final factor is O_3-Rich which has the highest explained variation for O_3. It accounts for 100% of O_3 in the winter and 75% in the summer. The other ancillary variables include CO, SO_2, BC, and $PM_{2.5}$ (28% and 48% for winter and summer, respectively). The profile typically has multiple modes with a small winter peak in the 10–20 nm range, the largest mode centered at 47 nm, and third mode at 170 nm. Summer has a similar small nucleation size mode, but the largest mode was the 170 nm mode representing more PM mass, and a relatively small mode at 37 nm.

Similar profiles were resolved in prior apportionments for Rochester (Ogulei et al., 2007a; Kasumba et al., 2009; Squizzato et al., 2019). Similar profiles have also been seen in most of the published PMF analyses of PNC data that included O_3 among the gaseous pollutants. For example, Sowlat et al. (2016) resolved a secondary aerosol profile in Los Angeles in which O_3 has the highest concentration, but the explained variation was not provided.

Given the strong relationship of the PNC with O_3, this source is thought to represent secondary particles that are likely to be organic in origin. O3 reacts with olefins such as terpenes to produce lower vapor pressure compounds that could then nucleate predominately in winter or condense on preexisting particles more in the warmer months to produce the observed multimodal distributions. However, the exact nature of the source(s) is not certain. There is a drop beginning in late 2007 and 2008 that could be related to the closing of the 260 MW coal-fired power plant on the northwestern side of Rochester whose effect had been observed in earlier studies (Jeong et al., 2004).

4. Conclusions

There were clear reductions in the PNC that were related to motor vehicles particularly with respect to the mandated reductions in fuel S content. These results suggest that the Tier II rules for light-duty vehicles, the heavy-duty diesel rules, and the non-road diesel fuel S content rules have had a definite effect on reducing PNCs in Rochester. Although it appears the new particle formation events declined for most of the study period, nucleation mode particles are increasing in recent years

likely due to the reduction of the condensational sink provided by accumulation mode particles. There were sudden drops in the two accumulation mode factors that were identified as secondary inorganic particles. These declines came in different years and the exact nature of these major changes are not known. However, both of these factors represent relatively low concentration contributions and thus, are subject to greater uncertainty. The particles associated with ambient O_3 concentrations remained fairly constant across the period. It may be that the increases in ambient O_3 concentrations have counteracted the declines in reactive precursors that form these particles.

CRediT authorship contribution statement

Philip K. Hopke: Writing – original draft, Supervision, Methodology, Investigation, Formal analysis, Data curation, Conceptualization. **Yunle Chen:** Writing – review & editing, Visualization, Formal analysis. **David C. Chalupa:** Writing – review & editing, Investigation, Data curation. **David Q. Rich:** Writing – review & editing, Supervision, Funding acquisition.

Declaration of competing interest

The authors declare that they have no known competing financial interests or personal relationships that could have appeared to influence the work reported in this paper.

Data availability

Data will be made available on request.

Acknowledgments

This work was supported by the New York State Energy Research and Development Authority (NYSERDA) Contracts #125993 and #156226. We would like to thank the New York State Department of Environmental Conservation and their staff for providing access to their monitoring site to house our SMPS and providing the black carbon data we have utilized in these analyses.

Appendix A. Supplementary data

Supplementary data to this article can be found online at https://doi.org/10.1016/j.envpol.2024.123708.

References

Carslaw, D.C., Ropkins, K., 2012. Openair - an R package for air quality data analysis. Environ. Model. Software 27–28, 52–61.

Chen, Y., Masiol, M., Squizzato, S., Chalupa, D.C., Zíková, N., Pokorná, P., Rich, D.Q., Hopke, P.K., 2022. Long-term trends of ultrafine and fine particle number concentrations in New York State: apportioning between emissions and dispersion. Environ. Pollut. 310, 119797.

Chen, Y., Rich, D.Q., Masiol, M., Hopke, P.K., 2023. Changes in ambient air pollutants in New York State from 2005 to 2019: effects of policy implementations and economic and technological changes. Atmos. Environ. 311, 119996.

Chen, Y., Rich, D.Q., Hopke, P.K., 2024. Changes in source specific $PM_{2.5}$ from 2010 to 2019. In: New York and New Jersey Identified by Dispersion Normalized PMF. Atmos, Res (under revision for resubmission).

Cleveland, R.B., Cleveland, W.S., McRae, J.E., Terpenning, I., 1990. STL: a seasonal-trend decomposition procedure based on loess. J. Off. Stat. 6 (1), 3–73.

Dai, Q., Liu, B., Bi, X., Wu, J., Liang, D., Zhang, Y., Feng, Y., Hopke, P.K., 2020. Dispersion normalized PMF provides insights into the significant changes in source contributions to PM2.5 after the COVID-19 outbreak. Environ. Sci. Technol. 54, 9917–9927.

Dai, Q., Ding, J., Hou, L., Li, L., Cai, Z., Liu, B., Song, C., Bi, X., Wu, J., Zhang, Y., Feng, Y., Hopke, P.K., 2021a. Haze episodes before and during the COVID-19 shutdown in Tianjin, China: contribution of fireworks and residential burning. Environ. Pollut. 286, 117252.

Dai, Q., Ding, J., Song, C., Liu, B., Bi, X., Wu, J., Zhang, Y., Feng, Y., Hopke, P.K., 2021b. Changes in source contributions to particle number concentrations after the COVID-19 outbreak: insights from a dispersion normalized PMF. Sci. Total Environ. 759, 143548.

Hopke, P.K., Feng, Y., Dai, Q., 2022. A source apportionment of particle number concentrations: a global review. Sci. Total Environ. 22, 1–5. https://doi.org/10.1016/j.scitotenv.2022.153104.

Hopke, P.K., Chen, Y., Rich, D.Q., Mooibroek, D., Sofowote, U.M., 2023. The application of positive matrix factorization with diagnostics to BIG DATA. Chemometr. Intell. Lab. Syst. 240, 104885.

Jeong, C.-H., Hopke, P.K., Chalupa, D., Utell, M., 2004. Characteristics of nucleation and growth events of ultrafine particles. Environ. Sci. Technol. 38, 1933–1940.

Jeong, C.-H., Evans, G.J., Hopke, P.K., Chalupa, D., Utell, M., 2006. Influence of atmospheric dispersion and new particle formation events on ambient particle number concentration in Rochester, USA and Toronto, Canada. J. Air Waste Manage. Assoc. 56, 431–443.

John, W., Wall, S.M., Ondo, J.L., Winklmayr, W., 1990. Modes in the size distributions of atmospheric inorganic aerosol. Atmos. Environ. 24, 2349–2359.

Kasumba, J., Hopke, P.K., Chalupa, D.C., Utell, M.J., 2009. Comparison of sources of submicron particle number concentrations measured at two sites in Rochester, NY. Sci. Total Environ. 407, 5071–5084.

Kittelson, D.B., Watts, W.F., Johnson, J.P., 2002. Diesel aerosol sampling methodology. Available at:. In: CRC E-43 Final Report. NTIS Accession No. PB2003-102418l. Available from CRC, Alpharetta, GA, p. 181 http://www.crcao.com/.

Kittelson, D.B., Watts, W.F., Johnson, J.P., 2004. Nanoparticle emissions on Minnesota highways. Atmos. Environ. 38, 9–19.

Kittelson, D.B., Watts, W.F., Johnson, J.P., 2006a. On-road and laboratory evaluation of combustion aerosols—part1: summary of diesel engine results. J. Aerosol Sci. 37, 913–930.

Kittelson, D.B., Watts, W.F., Johnson, J.P., Schauer, J.J., Lawson, D.R., 2006b. On-road and laboratory evaluation of combustion aerosols—Part 2: summary of spark ignition engine results. J. Aerosol Sci. 37, 931–949.

Masiol, M., Squizzato, S., Chalupa, D.C., Utell, M.J., Rich, D.Q., Hopke, P.K., 2018. Long-term trends in submicron particle concentrations in a metropolitan area of the northeastern United States. Sci. Total Environ. 633, 59–70, 2018.

McMurry, P.H., Friedlander, S.K., 1979. New particle formation in the presence of an aerosol. Atmos. Environ. 13, 1635–1651.

Muggeo, V.M.R., 2003. Estimating regression models with unknown break-points. Stat. Med. 22 (19), 3055–3071. https://doi.org/10.1002/sim.1545.

Muggeo, V.M.R., 2008. Segmented: an R package to fit regression models with broken-line relationships. R. News 8 (May), 20–25. https://doi.org/10.1159/000323281.

National Centers for Environmental Information (NCEI), 2023. Integrated Surface Dataset (Global). https://www.ncei.noaa.gov/access/search/data-search/global-hourly.

Oberdörster, G., Ferin, J., Gelein, R., Soderholm, S.C., Finkelstein, J., 1992. Role of the alveolar macrophage in lung injury: studies with ultrafine particles. Environ. Health Perspect. 97, 193–199, 1992.

Ogulei, D., Hopke, P.K., Chalupa, D.C., 2007a. Utell, M.J. Modeling source contributions to submicron particle number concentrations measured in rochester, New York. Aerosol Sci. Technol. 41, 179–201.

Ogulei, D., Hopke, P.K., Ferro, A.R., Jaques, P.A., 2007b. Factor analysis of submicron particle size distributions near a major United States-Canada trade bridge. J. Air Waste Manag. Assoc. 57, 190–203.

Paatero, P., 1999. The Multilinear Engine: a table-driven, least squares program for solving multilinear problems, including the n-way parallel factor analysis model. J. Comput. Graph Stat. 8, 854–888.

Paatero, P., Eberly, S., Brown, S.G., Norris, G.A., 2014. Methods for estimating uncertainty in factor analytic solutions. Atmos. Meas. Tech. 7, 781–797.

Polissar, A.V., Hopke, P.K., Paatero, P., Malm, W.C., Sisler, J.F., 1998. Atmospheric aerosol over Alaska: 2. Elemental composition and sources. J. Geophys. Res. Atmos. 103, 19045–19057.

Preble, C.V., Harley, R.A., Kirchstetter, T.W., 2019. Control technology-driven changes to in-use heavy-duty diesel truck emissions of nitrogenous species and related environmental impacts. Environ. Sci. Technol. 53, 14568–14576.

Sen, P.K., 1968. Estimates of the regression coefficient based on Kendall's Tau. J. Am. Stat. Assoc. 63 (324), 1379–1389. https://doi.org/10.2307/2285891.

Squizzato, S., Masiol, M., Rich, D.Q., Hopke, P.K., 2018. PM2.5 and gaseous pollutants in New York State during 2005–2016: spatial variability, temporal trends, and economic influences. Atmos. Environ. 183, 209–224.

Squizzato, S., Masiol, M., Emami, F., Chalupa, D.C., Utell, M.J., Rich, D.Q., Hopke, P.K., 2019. Long-term changes of source apportioned particle number concentrations in a metropolitan area of the northeastern United States. Atmosphere 10, 27.

Sowlat, M.H., Hasheminassab, S., Sioutas, C., 2016. Source apportionment of ambient particle number concentrations in central Los Angeles using positive matrix factorization (PMF). Atmos. Chem. Phys. 16, 4849–4866.

Sun, Y.L., Zhang, Q., Schwab, J.J., Chen, W.N., Bae, M.S., Lin, Y.C., Hung, H.M., Demerjian, K.L., 2011. A case study of aerosol processing and evolution in summer in New York City. Atmos. Chem. Phys. 11, 12737–12750.

Theil, H., 1950. A rank-invariant method of linear and polynomial regression analysis. Proceed. Royal Netherlands. Acad. Sci. 53, 386–392. https://doi.org/10.1007/978-94-011-2546-8_20.

Trechera, P., Garcia-Marlès, M., Liu, X., Reche, C., Pérez, N., Savadkoohi, M., Beddows, D., Salma, I., Vörösmarty, M., Casans, A., Casquero-Vera, J.A., Hueglin, C., Marchand, N., Chazeau, B., Gille, G., Kalkavouras, P., Mihalopoulos, N., Ondracek, J., Zikova, N., Niemi, J.V., Manninen, H.E., Green, D.C., Tremper, A.H., Norman, M., Vratolis, S., Eleftheriadis, K., Gómez-Moreno, F.J., Alonso-Blanco, E., Gerwig, H., Wiedensohler, A., Weinhold, K., Merkel, M., Bastian, S., Petit, J.E., Favez, O., Crumeyrolle, S., Ferlay, N., Martins Dos Santos, S., Putaud, J.-P., Timonen, H., Lampilahti, J., Asbach, C., Wolf, C., Kaminski, H., Altug, H., Hoffmann, B., Rich, D.Q., Pandolfi, M., Harrison, R.M., Hopke, P.K., Petäjä, T.,

Alastuey, A., Querol, X., 2023. Phenomenology of ultrafine particle concentrations and size distribution across urban Europe. Environ. Int. 172, 107744 https://doi.org/10.1016/j.envint.2023.107744.
Uria-Tellaetxe, I., Carslaw, D.C., 2014. Conditional bivariate probability function for source identification. Environ. Model. Software 59, 1–9.
United States Environmental Protection Agency (USEPA), 2023. https://www.epa.gov/power-sector/progress-report-emissions-reductions#so2. https://www.epa.gov/power-sector/progress-report-emissions-reductions#nox.
Utell, M.J., Frampton, M.W., 2002. Acute health effects of ambient air pollution: the ultrafine particle hypothesis. J. Aerosol Med. 13, 355–359.
Wang, Y., Hopke, P.K., Chalupa, D.C., Utell, M.J., 2011a. Long-term study of urban ultrafine particles and other pollutants. Atmos. Environ. 45 (40), 7672–7680.
Wang, Y., Hopke, P.K., Rattigan, O.V., Xia, X., 2011b. Characterization of residential wood combustion particles using the two-wavelength aethalometer. Environ. Sci. Technol. 45, 7387–7393.
Wang, M., Hopke, P.K., Masiol, M., Thurston, S.W., Cameron, S., Ling, F., van Wijngaarden, E., Croft, D., Squizzato, S., Thevenet-Morrison, K., Chalupa, D., Rich, D.Q., 2019. Changes in triggering of ST-elevation myocardial infarction by particulate air pollution in Monroe County, New York over time: a case-crossover study. Environ. Health 18, 82.
Wang, M., Kong, W., Marten, R., et al., 2020. Rapid growth of new atmospheric particles by nitric acid and ammonia condensation. Nature 581, 184–189.
World Health, Organization., 2021. WHO Global Air Quality Guidelines. Particulate Matter (PM2.5 and PM10), Ozone, Nitrogen Dioxide, Sulfur Dioxide and Carbon Monoxide. World Health Organization, Geneva.
Yang, K., Fox, J.T., Hunsicker, R., 2016. Characterizing diesel particulate filter failure during commercial fleet use due to pinholes, melting, cracking, and fouling. Emiss. Control Sci. Technol. 2, 145–155.
Yount, C.S., Utell, M.J., Hopke, P.K., Thurston, S.W., Lin, S., Ling, F.S., Chen, Y., Chalupa, D., Deng, X., Rich, D.Q., 2023. Triggering of ST-elevation myocardial infarction by ultrafine particles in New York: Changes following Tier 3 vehicle introduction. Environ. Res. 216, 114445.
Zhao, Y.L., Hennigan, C.J., May, A.A., Tkacik, D.S., de Gouw, J.A., Gilman, J.B., Kuster, W.C., Borbon, A., Robinson, A.L., 2014. Intermediate-volatility organic compounds: a large source of secondary organic aerosol. Environ. Sci. Technol. 48, 13743–13750.
Zhao, Y., Nguyen, N.T., Presto, A.A., Hennigan, C.J., May, A.A., Robinson, A.L., 2015. Intermediate volatility organic compound emissions from on-road diesel vehicles: chemical composition, emission factors, and estimated secondary organic aerosol production. Environ. Sci. Technol. 49, 11516–11526.
Zhao, Y., Nguyen, N.T., Presto, A.A., Hennigan, C.J., May, A.A., Robinson, A.L., 2016. Intermediate volatility organic compound emissions from on-road gasoline vehicles and small off-road gasoline engines. Environ. Sci. Technol. 50, 4554–4563.
Zhao, Y., Lambe, A.T., Saleh, R., Saliba, G., Robinson, A.L., 2018. Secondary organic aerosol production from gasoline vehicle exhaust: effects of engine technology, cold start, and emission certification standard. Environ. Sci. Technol. 52, 1253–1261.
Zhou, L., Kim, E., Hopke, P.K., Stanier, C.O., Pandis, S., 2004. Advanced factor analysis on Pittsburgh particle size-distribution data. Aerosol. Sci. Technol. 38 (S1), 118–132.
Zhou, L., Hopke, P.K., Stanier, C.O., Pandis, S.N., Ondov, J.M., Pancras, J.P., 2005. Investigation of the relationship between chemical composition and size distribution of airborne particles by partial least squares (PLS) and positive matrix factorization (PMF). J. Geophys. Res. 110, D07S18.